

Discrete multi-material topology optimization under total mass constraint

Xingtong Yang, Ming Li*

State Key Laboratory of CAD&CG, Zhejiang University, Hangzhou, China

ARTICLE INFO

Keywords:

Multi-material
Topology optimization
Discrete solution
Total mass constraint
Theoretical proof

ABSTRACT

A novel approach to computing the discrete solution to the challenging multi-material topology optimization problem under total mass constraint is studied in this paper. The challenge of the problem lies in the incompressibility constraint on the summation of the usage of the total materials, which significantly increases the associated computational difficulty, and is seldom studied before; a few previous studies focus on respective mass constraint on each used material, whose solution lies in a strictly feasible space and is easier to compute. Solution to the optimization problem is derived on a theoretical finding that the iterative density update in a two-material optimization problem is totally determined by the rankings of the elemental compliances, which only involves an FE analysis computation, and can be efficiently achieved. Based on this theoretical insight, a practical *regulated* iterative numerical approach is then devised to find the solution to the multi-material topology optimization problem by solving a series of two-material subproblems. Various 2D and 3D numerical examples demonstrate its capability in providing structure of better compliance as compared with results obtained using latest approach based on density interpolation.

© 2018 Elsevier Ltd. All rights reserved.

1. Introduction

Topology optimization finds the best material distribution within a prescribed design domain, solid or void, in order to produce a structure of optimal performance. Since the seminar work by Bendsoe and Kikuchi [1], topology optimization has undergone a remarkable development over the past decades in both academic research [2–5] and industrial applications [6,7]. Amongst these developments, most of these approaches generally relaxed the problem into a continuous parameter optimization problem taking elemental density (such as SIMP (Solid Isotropic Material with Penalization) [8]) or structural outer shape as design variables (such as level set [9,10]), and then solve it based on the traditional Newton-type (gradient-based) optimization algorithms. Other researches also compute directly discrete solutions to the problem using evolutionary approach (such as BESO (Bi-directional Evolutionary Structural Optimization) [11,12]) or programming techniques [13]. A comprehensive comparison between these approaches are referred to a recent survey [14,3].

In the single-material topology optimization, the material is specified a-priori and the structure is optimized with respect to it. In contrast, the multi-material topology optimization is posed to seek not only the optimal structural form but also simultaneously

various material distributions, in order to realize specific design purposes that are otherwise difficult to achieve by single-material structures [15], or to achieve optimal structural performance. As compared with the widely studied former problem, the latter one is much less studied, including approaches based on density (SIMP) [16], phase field [17–19], level set [20], combinatorial optimization [21], or evolutionary approach (BESO) [22]. A recent detailed discussions on the topic are further referred to [19,16].

Challenges. The challenges of multi-material topology optimization are mainly related to its intrinsic mathematical structure of the design space. In the case of single material, the design variable is just the occupation of the single material, whose associated design space is generally sufficiently regular, and can be easily resolved for instance using the optimality criteria [23] or gradient projection [18,19] methods; using discrete variables is only studied by [21]. In contrast, in the case of multi-materials on *total mass* constraint, an additional usage on the summation of the total materials (the incompressibility constraint) is required, which significantly increases the computational costs of the corresponding numerical solution, which is seldom studied before [24–26,21,16].

The different mathematical structures additionally raise challenging issues on an appropriate topology description model, which has to effectively indicate distinct materials inside the domain, fully covering the design domain but not overlapping. Specifically, each elemental domain has a distinct material and they all

* Corresponding author.

E-mail address: liming@cad.zju.edu.cn (M. Li).

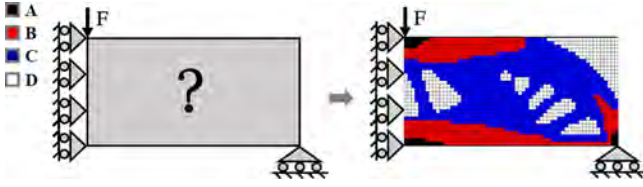


Fig. 1. An example of four-material topology optimization problem. A, B, C and D are four kinds of candidate materials with different Young's modulus and densities.

together, materials and voids, fully cover the design domain. Previous approaches based on density or shape descriptions and interpolation have to carefully devise various strategies to overcome it, and also have a risk of having intermediate design elements with nonphysical materials. The proposed discrete optimization approach naturally avoids these issues.

Approach and contributions. The paper proposes a novel approach to multi-material topology optimization under *total mass* constraint, only studied previously in [21,16] to our best knowledge. The proposed approach is also the first using discrete variables to resolve the multi-material optimization problem under total mass constraint. The discrete variable representation thus avoids the limitations of previous interpolation-based approaches in that they are not physically based or have intermediate design elements. Furthermore, the discrete material expression naturally satisfies the design requirements that all the material densities are separated and fully occupy the design domain.

The overall approach is based on an evolutionary mass reduction strategy, and focuses on the classical compliance minimization problem. The success of the approach is built on a key observation under rigorous proof that the optimal material distribution update in each iteration step only depends on the elemental compliance ranking in case of two materials, and cases of multi-material can be reduced to the two-material problem. The convergence of the overall approach is further improved via introducing a *density regulation* approach that ensures smooth density transition during the optimization process. Performance of the proposed approach is demonstrated through 2D and 3D numerical examples. Its comparisons with results obtained using classical SIMP approach shows its capability in designing structures of better compliance.

The remainder of the paper is arranged as follows. Problem definition and the theoretical basis to resolve it are given in Section 2. Section 3 explains technical details on its numerical implementation. Numerical results on 2D and 3D examples are demonstrated in Section 4, and the paper is concluded in Section 5.

2. Problem and theory

Suppose $\Omega = \{\Omega_e, e = 1 \dots N\}$ is a discrete design domain consisting of N disjoint square FE elements $\Omega_e, (E_j, \rho_j), j = 1 \dots m$ are the m candidate materials of Young's modulus E_j and density ρ_j satisfying $E_1 \geq \dots \geq E_m$ and $\rho_1 \geq \dots \geq \rho_m$; it is assumed that all the base materials have equal Poisson's ratios. Apparently, for candidate materials satisfying $E_i \geq E_j, \rho_i \leq \rho_j$, material i is just superior to material j in problem (1), and we can simply choose material i instead of j without further topology optimization.

The multi-material topology optimization problem considers the classical problem of maximizing the stiffness of a structure, or minimizing its compliance under constraint on the usage of total mass, as illustrated in Fig. 1 and stated below. Find the optimal multi-material distribution \mathbf{x} such that

$$\begin{aligned} \min_{\mathbf{x}} \quad & c(\mathbf{x}) = \frac{1}{2} \mathbf{u}^T \mathbf{K}(\mathbf{x}) \mathbf{u} \\ \text{s.t.} \quad & \mathbf{K}(\mathbf{x}) \mathbf{u} = \mathbf{f}, \mathbf{u} \in \mathcal{U} \\ & M(\mathbf{x}) \leq M^*. \end{aligned} \quad (1)$$

Here \mathbf{x} gives the specific material of every finite element as

$$\mathbf{x} = \{\mathbf{x}_e\}, \mathbf{x}_e = \{x_{ej}\}, e = 1, \dots, N, j = 1, \dots, m, \quad (2)$$

where $x_{ej} = 1$ or 0 determines whether element e is filled with the j th material at an addition requirement that each element e is filled by one and only one kind of material, that is,

$$\sum_{j=1}^m x_{ej} = 1. \quad (3)$$

The total mass is defined as follows

$$M(\mathbf{x}) = \sum_{e=1}^N \rho(\mathbf{x}_e), \text{ for } \rho(\mathbf{x}_e) = \sum_{j=1}^m x_{ej} \rho_j. \quad (4)$$

In addition, \mathbf{u} and $\mathcal{U} \subset \mathbb{R}^N$ are the nodal displacement vector and its admissible space, where certain Dirichlet boundary conditions are prescribed. $\mathbf{K}(\mathbf{x})$ is the global stiffness matrix, decided by material distribution \mathbf{x} , which is calculated by

$$\mathbf{K}(\mathbf{x}) = \{E(\mathbf{x}_e) \mathbf{k}_0\}, E(\mathbf{x}_e) = \sum_{j=1}^m x_{ej} E_j \quad (5)$$

for a unit stiffness matrix \mathbf{k}_0 . \mathbf{f} is the external force vector. The structure compliance $c(\mathbf{x})$ is calculated by

$$c(\mathbf{x}) = \frac{1}{2} \mathbf{u}^T \mathbf{K}(\mathbf{x}) \mathbf{u} = \sum_{e=1}^N \sum_{j=1}^m \frac{1}{2} x_{ej} E_j \mathbf{u}_e^T(\mathbf{x}) \mathbf{k}_0 \mathbf{u}_e(\mathbf{x}), \quad (6)$$

where \mathbf{u}_e is the displacement vector of element e .

The original problem (1) is equivalently written

$$\min_{\mathbf{x} \in \mathcal{A}} \{c(\mathbf{x}) \mid \mathbf{K}(\mathbf{x}) \mathbf{u} = \mathbf{f}\}, \quad (7)$$

where the design domain $\mathcal{A} = \{\mathbf{x} \mid M(\mathbf{x}) \leq M^*\}$.

The proposed approach to resolving problem (1) is achieved via gradually reducing the mass from an initial distribution till the target one, as also used in the well-studied evolutionary approach BESO [27]. The initial value of \mathbf{x} is set as density fully filled by the material M^1 of the largest Young's modulus among all the candidate materials, which is an obvious global optimal solution under the associated mass constraint. Before further explanation on the overall approach, we first explain below the density update strategy in each of the optimization step as the base of the proposed approach.

Noticing that the stiffness matrix \mathbf{K} and displacement \mathbf{u} are both dependent on the density \mathbf{x} , taking derivatives on both sides of the equilibrium equation

$$\mathbf{K}(\mathbf{x}) \mathbf{u}(\mathbf{x}) = \mathbf{f} \quad (8)$$

with respect to the design variable x_{ej} gives

$$\frac{\partial \mathbf{K}(\mathbf{x})}{\partial x_{ej}} \mathbf{u}(\mathbf{x}) + \mathbf{K}(\mathbf{x}) \frac{\partial \mathbf{u}(\mathbf{x})}{\partial x_{ej}} = 0, \quad (9)$$

and by basic transformation, there is

$$\frac{\partial \mathbf{u}(\mathbf{x})}{\partial x_{ej}} = -\mathbf{K}^{-1}(\mathbf{x}) \frac{\partial \mathbf{K}(\mathbf{x})}{\partial x_{ej}} \mathbf{u}(\mathbf{x}). \quad (10)$$

On the other hand, according to the compliance definition and equilibrium equation (8)

$$c(\mathbf{x}) = \frac{1}{2} \mathbf{u}^T \mathbf{K}(\mathbf{x}) \mathbf{u}(\mathbf{x}) = \frac{1}{2} \mathbf{u}^T(\mathbf{x}) \mathbf{f}, \quad (11)$$

we have its partial derivative with respect to design variable x_{ej}

$$\frac{\partial c(\mathbf{x})}{\partial x_{ej}} = \frac{1}{2} \mathbf{f}^T \frac{\partial \mathbf{u}}{\partial x_{ej}}, \quad (12)$$

which is further written, by using (8) (10), as

$$\frac{\partial c(\mathbf{x})}{\partial x_{ej}} = -\frac{1}{2} \mathbf{u}^T \frac{\partial \mathbf{K}}{\partial x_{ej}} \mathbf{u} = -\frac{1}{2} x_{ej} E_j \mathbf{u}_e^T(\mathbf{x}) \mathbf{k}_0 \mathbf{u}_e(\mathbf{x}) = -c(x_{ej}) \quad (13)$$

where the component-wise of $c(\mathbf{x})$ is

$$c(x_{ej}) = \frac{1}{2} x_{ej} E_j \mathbf{u}_e^T(\mathbf{x}) \mathbf{k}_0 \mathbf{u}_e(\mathbf{x}). \quad (14)$$

Besides, the elemental compliance $c(\mathbf{x})_e$ is

$$c(\mathbf{x})_e = \sum_{j=1}^m c(x_{ej}). \quad (15)$$

With the above preparations, we further derive below the density update from total M^1 to M^2 for $M^2 < M^1$ and close enough. Specifically, given mass fractions M^1, M^2 , and the corresponding optimized material distribution \mathbf{x}^{M^1} , we hope to update \mathbf{x}^{M^1} to \mathbf{x}^{M^2} to minimize the structure compliance at mass constraint M^2 . According to Taylor expansion, the objective function is approximately expressed as

$$\begin{aligned} c(\mathbf{x}^{M^2}) &= c(\mathbf{x}^{M^1} - (\mathbf{x}^{M^1} - \mathbf{x}^{M^2})) \\ &= c(\mathbf{x}^{M^1}) - c'(\mathbf{x}^{M^1})(\mathbf{x}^{M^1} - \mathbf{x}^{M^2}) + O(\mathbf{x}^{M^1} - \mathbf{x}^{M^2}) \\ &\approx c(\mathbf{x}^{M^1}) - c'(\mathbf{x}^{M^1})(\mathbf{x}^{M^1} - \mathbf{x}^{M^2}). \end{aligned} \quad (16)$$

In this situation, the minimizing problem in (7) becomes

$$\begin{aligned} \arg \min c(\mathbf{x}^{M^2}) &= \arg \min c(\mathbf{x}^{M^2}) - c(\mathbf{x}^{M^1}) \\ &\approx \arg \min -c'(\mathbf{x}^{M^1})^T (\mathbf{x}^{M^1} - \mathbf{x}^{M^2}). \end{aligned} \quad (17)$$

Further taking into account of (13) and noticing that \mathbf{x}^{M^1} is constant, the above equation gives

$$\begin{aligned} \arg \min c(\mathbf{x}^{M^2}) &\approx \arg \min c(\mathbf{x}^{M^1})^T (\mathbf{x}^{M^1} - \mathbf{x}^{M^2}) \\ &= \arg \min -c(\mathbf{x}^{M^1})^T \mathbf{x}^{M^2} \\ &= \arg \max c(\mathbf{x}^{M^1})^T \mathbf{x}^{M^2}. \end{aligned} \quad (18)$$

Consequently, we have an equivalent optimization problem to (7) at a local region around \mathbf{x}^{M^1} ,

$$\max_{\mathbf{x}} \{c(\mathbf{x}^{M^1})^T \mathbf{x} \mid \mathbf{K}(\mathbf{x}) \mathbf{u} = \mathbf{f}, M(\mathbf{x}) \leq M^2\}, \quad (19)$$

that is, it is reasonable to solve the optimization problem via approximately maximizing $c(\mathbf{x}^{M^1})^T \mathbf{x}$, starting from the known optimal solution \mathbf{x}^{M^1} .

The above problem is a typical grouping knapsack problem, whose solution is usually computed using dynamic planning approaches. However, the complexity of this method is severely restricted by the size of the problem. In practice, even for a medial size problem, the computational cost is almost unaffordable. An alternative strategy is proposed in this paper, which is relatively acceptable and efficient, based on the characteristic of the problem itself.

The proposed approach is based on the observation that in case of two-material, the mass constraint, together with the constraint on the number of total elements, strictly determines the numbers of the two materials. Once the number determined, solution to the problem (19) in case of two-materials is totally determined by the elemental compliance rankings. The result is summarized in the lemma below; also depicted in Fig. 2.

Lemma 1. Let \mathbf{x}^{M^1} be an optimal solution to problem (1) under mass bound M^1 , and M^2 be another mass bound satisfying $M^1 \geq M^2$, $|M^1 - M^2| \leq \delta$, $\delta > 0$. Then the solution to problem (1) under mass bound M^2 can be approximatively solved by

$$\max_{\mathbf{x}} c(\mathbf{x}^{M^1})^T \mathbf{x}^{M^2}, \quad (20)$$

whose solution can be easily determined by choosing the top elements of bigger compliances $c(\mathbf{x}^{M^1})_e$ whose sum of masses is less than M^2 . In addition, the obtained solution is the best solution to problem (19).

Proof. See Appendix.

Based on the above result, in order to successfully handle the general case of m -materials, where $m > 2$, we can reduce the problem into a series of two-material problem via iterating all the possible material combinations. Due to the constraints on the total mass and the number of design elements, the iteration number can be confined within a relatively small range.

The overall approach is summarized in the left in Fig. 3, where Ω_j ($j = 1, \dots, m-2$) prescribes the range of all the possible numbers of certain material, confined by the usage of total mass and the number of design elements. The iteration starts from an initial density, fully filled with material m_1 of highest Young's modulus, at default total mass M^1 . It then iteratively reduces the target total mass from M^i to M^{i+1} within all possible material ranges $\Omega^{i+1} = \Omega_1 \times \dots \times \Omega_m$. The process reduces the multi-material problem into a series of two-material problem. The iteration repeats until reaching the target mass and satisfying certain stopping criteria.

In addition, each iteration process of each sub-loop all involves a novel *density regulation* process for optimization convergence control. It involves stages of preprocessing, upward and downward searching. The preprocessing stage transfers the current optimized multi-material density into another proper density in the density range for usage in the next iteration. The upward and downward stages searches the best density for all the possible material combinations from the current optimized one.

3. Numerical approach

This section gives the technical details of implementing the proposed strategy, including two-material problem and more-than-two-material problems, which are arranged from easy to difficult. For further explanation, the latter is illustrated by three-material and four-material problems separately.

3.1. Two-material problem

In case of two materials, the structure is only composed of N elements and satisfies the total mass constraint, prescribing

$$\begin{cases} n_1 + n_2 = N \\ n_1 \rho_1 + n_2 \rho_2 \leq M^* \end{cases} \Rightarrow \begin{cases} n_1 \leq \frac{M^* - N \rho_2}{\rho_1 - \rho_2} \\ n_2 = N - n_1 \end{cases} \quad (21)$$

where n_i is the number of elements filled with material i .

Supposing $E_1 \geq E_2$, $\rho_1 \geq \rho_2$, we accordingly have the number of material 1 and 2, that is n_1 and n_2 is set to be

$$n_1 = \lfloor \frac{M^* - N \rho_2}{\rho_1 - \rho_2} \rfloor, n_2 = N - n_1. \quad (22)$$

The whole procedure of two-material optimization is outlined below:

Step 1: Input material properties, total mass constraint M^* , evolutionary ratio ER , domain size n_{elx} , n_{ely} , and initial density consisting of only material 1.

Step 2: Set the next target mass as follows

$$M^{i+1} = \max(M^i(1 - ER), M^*). \quad (23)$$

Step 3: Calculate elemental compliances $\{c_e^{M^i}\}$ via (14), (15) via FE analysis.

Step 4: Determine the number of materials 1 and 2 in the design domain

$$n_1 = \lfloor \frac{M^{i+1} - N \rho_2}{\rho_1 - \rho_2} \rfloor, n_2 = N - n_1. \quad (24)$$

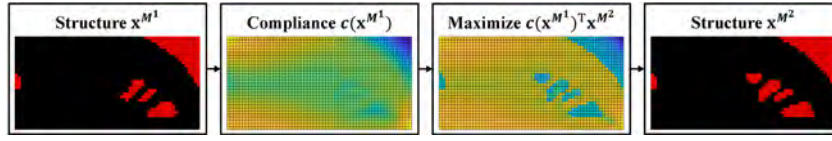


Fig. 2. Illustration of Lemma 1. From left to right, the first figure shows the input structure \mathbf{x}^{M^1} satisfying mass constraint M^1 . The second shows the value of $c(\mathbf{x}^{M^1})$. The third shows the resulted density after maximizing $c(\mathbf{x}^{M^1})^T \mathbf{x}^{M^2}$. The last shows the optimized structure \mathbf{x}^{M^2} under mass constraint M^2 as output.

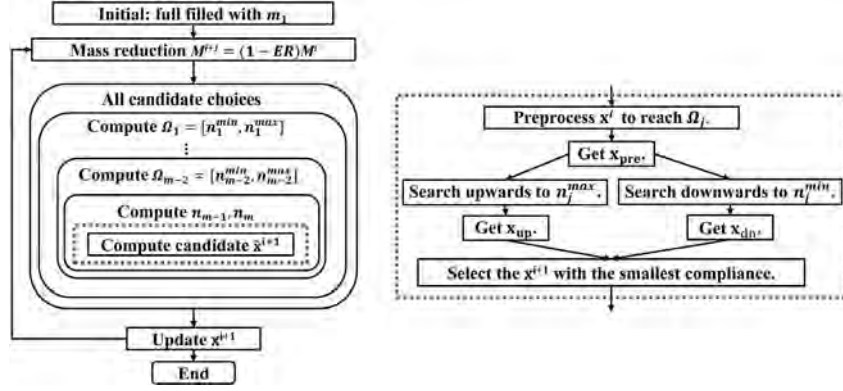


Fig. 3. Overview of the proposed approach. The left illustrates the main mass deduction process and an iteration in searching for all the possible numbers of materials, which ultimately reduces the multi-material optimization problem to a series of two-material optimization problems. The right figure indicates the density regulation process for optimization convergence control.

Step 5: Update density \mathbf{x}^{i+1} via filling the top n_1 elements of large compliances $\{c_e^{M^i}\}$ by material 1, and others by material 2.

Step 6: Repeat steps 2–5 until the objective mass is achieved and the convergent criterion is satisfied

$$error = \frac{\|\mathbf{x}^{i+1} - \mathbf{x}^i\|}{\|\mathbf{x}^{i+1}\|} \leq \tau \quad (25)$$

In this paper, the superscript usually refers to the mass iteration, and the subscript denotes the finite element or a certain kind of material. In addition, various kinds of element-based filters can be added before step 4 [3].

We also comment here the difference between the proposed approach and the well-studied BESO [28]. Technically speaking, for two-material problem, the proposed method is pretty similar to BESO as the number of two materials are totally determined from the constraint on the total mass. However, the fundamental motives are rather different: BESO is heuristically based on elemental sensitivities, while the proposed is driven by the result in Lemma 1, which states the important role of the element number. This difference enables the proposed method to be extended to more-than-two-material problems easily and straightforward.

3.2. Three-material problem

For more-than-two-material problems, the main difficulty of applying Lemma 1 is that it is basically impossible to select the best amount of each material directly, because the bargain between any two materials is not independent. Noticing that in the case of three materials, once the number of one kind of material is decided, the numbers of the other two are correspondingly determined, noticing that their constraint on total mass and on element number. Therefore, a new relatively efficient traversal method is proposed to resolve the case of three-material problem via searching for the possible amount of each material. In addition, in order to achieve smoothness and stability of the optimization, pre-processing procedure is added at the beginning in each mass iteration, instead of setting \mathbf{x}^i as the initial value at mass M^{i+1} . What follows illustrates it in detail.

3.2.1. Basic idea

Since there are three kinds of materials to choose from, taking into account the mass and volume constraints, once the amount of any one among them is fixed, the rest two can be settled correspondingly. Furthermore, when a reasonable initial structure \mathbf{x}^{M^i} is given, the next new material distribution $\mathbf{x}^{M^{i+1}}$ can be obtained directly on the principle of maximizing $c(\mathbf{x}^{M^i})^T \mathbf{x}^{M^{i+1}}$ from Lemma 1.

The key problem here is to find the best quantity of each material. The strategy taken here is to loop over a relatively small set of possible material combinations, and choose the best one amongst them. It thus correspondingly reduces the three-material optimization problem to a series of two-material optimization problem.

Suppose there are three materials satisfying $E_1 \geq E_2 \geq E_3, \rho_1 \geq \rho_2 \geq \rho_3$ without loss of generality. Considering the mass constraint M^{i+1} in current iteration, the possible maximum number n_{1_max} of material 1 and the minimum n_{3_min} of material 3 can be calculated by

$$\begin{cases} n_1 + n_3 = N \\ n_1 \rho_1 + n_3 \rho_3 \leq M^{i+1} \end{cases} \Rightarrow \begin{cases} n_1 \leq \frac{M^{i+1} - N \rho_3}{\rho_1 - \rho_3} \\ n_3 = N - n_1 \end{cases}, \quad (26)$$

which gives the upper bound of n_1 and lower bound of n_3 as

$$n_{1_max} = \lfloor \frac{M^{i+1} - N \rho_3}{\rho_1 - \rho_3} \rfloor, \quad n_{3_min} = N - n_{1_max}. \quad (27)$$

Moreover, once given a mass constraint M^{i+1} and the number n_1 of material 1, the amount of the other two materials must satisfy

$$\begin{cases} n_2 + n_3 = N - n_1 \\ n_2 \rho_2 + n_3 \rho_3 \leq M^{i+1} - n_1 \rho_1 \end{cases}. \quad (28)$$

Considering material 2 is superior to material 3 in Young's modulus as $E_2 > E_3$, apply the main idea of two-material problem to (28), there gives

$$n_2 = \lfloor \frac{M^{i+1} - n_1 \rho_1 - (N - n_1) \rho_3}{\rho_2 - \rho_3} \rfloor, \quad n_3 = N - n_1 - n_2. \quad (29)$$

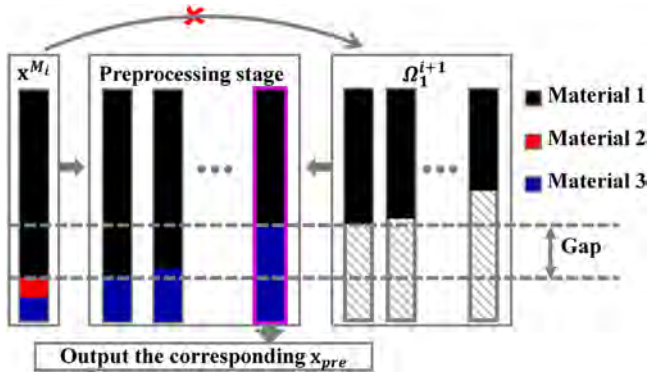


Fig. 4. Preprocessing stage of three-material problem.

Accordingly, in each mass deduction iteration, the proposed method will construct and search a set of feasible material combinations $\Omega = \Omega_1 \times \Omega_2 \times \Omega_3$, mainly confined by the feasible range $\Omega_1 = [n_{1_min}, n_{1_max}]$ of material 1. Ω_1 is the range for minimal and maximal allowable numbers of elements taken by material 1. In order for algorithm efficiency, we basically set the value of n_{1_min} as $0.9 \cdot n_{1_max}$ according to our experimental results.

Now the main issue left to be resolved is the search strategy of these combinations. To prevent an abrupt density variation during the iteration while meanwhile keeping efficient, this search step is further decomposed into three sub-iterations for clarity, including preprocessing iteration, upwards searching iteration and downwards searching iteration, as shown in the dashed frame in Fig. 3.

3.2.2. Preprocessing stage

The preprocessing stage aims to ensure a smooth density transition from the last best structure to a feature structure in its feasible region in the current iteration. The process neglects the total mass constraint tentatively.

Suppose we have an optimal density \mathbf{x}^i consisting of three materials respectively of number (n_1^i, n_2^i, n_3^i) in last main-loop iteration step at mass constraint M^i . We hope to update \mathbf{x}^i to \mathbf{x}^{i+1} at mass constraint M^{i+1} . Suppose the new feasible interval of material 1 is $\Omega_1 = [n_{1_min}, n_{1_max}]$ for mass constraint M^{i+1} . A pitfall here is that n_1^i may not be in Ω_1 . The preprocessing stage is designed here to regenerate a new density $\tilde{\mathbf{x}}^i \in \Omega_1$ following the procedure below.

The preprocessing step gradually find $\tilde{\mathbf{x}}^i \in \Omega_1$ via iterating different numbers of domain material compositions, specifically,

1. Moving from (n_1^i, n_2^i, n_3^i) at mass constraint M^i ,
2. via to an intermediate composition $(n_1^i, 0, N - n_1^i)$ at mass M^{i+1} ,
3. till reaching $(n_{1_max}, 0, N - n_{1_max})$ at mass M^{i+1} .

In each step of material number variations, the associated density distribution \mathbf{x} is found via the proposed optimization approach.

It is noted here that above preprocessing usually much improves the iteration stability, at a cost of additional FE analysis for density updating. The well-ensured convergence demonstrates its validity and worthwhile (see Fig. 4).

3.2.3. Upwards and downwards stage

Once the n_1 of an initial structure lies in Ω_1 , as described above, the best density distribution can be iteratively achieved via a two sub-iterations: upwards searching procedure from n_1 to n_{1_max} , and downwards searching procedure from n_1 to n_{1_min} . In this stage, n_1 is increased or decreased at certain, and the values of n_2

and n_3 are determined accordingly via (29). The structures with minimum c_{up} in upwards stage and c_{dn} in downwards are denoted \mathbf{x}_{up} and \mathbf{x}_{dn} , respectively. The best of them gives the next update density.

3.3. More-than-three-material problem

This above described approach is easily extended to optimization with more candidate materials. Suppose we have a four-material design problem with $E_i \geq E_{i+1}$ and $\rho_i \geq \rho_{i+1}$, for $i = 1, \dots, 3$, and the outer-most main-loop is determined by material 1. For a given n_1 and mass constraint M^i , the feasible region of n_2 to be searched is calculated by

$$n_{2_max} = \min(\lfloor \frac{M^i - n_1\rho_1 - (N - n_1)\rho_4}{\rho_2 - \rho_4} \rfloor, N - n_1), \tag{30}$$

and we set $n_{2_min} = 0.9n_{2_max}$ by default.

During each n_2 iteration, n_3 is calculated by

$$n_3 = \min(\lfloor \frac{M_3^i - n_2\rho_2 - (N_3 - n_2)\rho_4}{\rho_3 - \rho_4} \rfloor, N_3 - n_2), \tag{31}$$

where

$$M_3^i = M^i - n_1\rho_1, N_3 = N - n_1, \tag{32}$$

and $n_4 = N_3 - n_2 - n_3$.

Once the range of material composition determined, the above described preprocessing, upward and downward searching will also be conducted as similar as the case of three materials, and are not further explained here.

3.4. Termination criterion

The termination criterion is generally determined by the convergence of objective function or design variables, and the proposed approach is able to converge at this condition. On the other hand, various experiments also indicates that the optimal structures are usually found once the target mass constraint is satisfied. The criteria is thus taken in practical experiments to save computational costs.

3.5. Filter scheme

In order to avoid numerical instabilities such as checkerboard and mesh-dependency, various filters can be applied here following previous studies in [22,23,27]. The filter applied here is mainly designed based on computing an elemental compliance c_i via averaging those around it within a length scale r_{min} , or specifically,

$$\hat{c}_i = \frac{\sum_{j=1}^S w(r_{ij})c_j}{\sum_{j=1}^N w(r_{ij})}, \tag{33}$$

where S is the total number of nodes involved, and r_{ij} denotes the distance between the center of the element i and node j , and $w(r_{ij})$ is a weight factor given as

$$w(r_{ij}) = \begin{cases} r_{min} - r_{ij} & \text{for } r_{ij} < r_{min} \\ 0 & \text{for } r_{ij} \geq r_{min}. \end{cases} \tag{34}$$

The filter is specifically involved in the following stages: each step after a preprocessing, and each step after generating an optimal structure in each mass reduction process in the main iteration-loop.

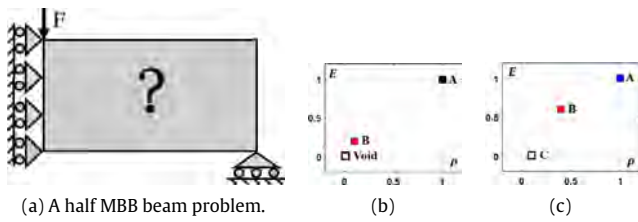


Fig. 5. Problem definition and candidate materials. (b) Materials in Section 4.1. (c) Materials in Section 4.2.

4. Numerical examples

The proposed approach has been implemented in Matlab, and run on a PC of Intel Core i5-4590 of 3.2 GHz CPU and 16GB RAM. Its performance is tested on various 2D and 3D examples. Specifically, the two-material case is the base of the approach and is first tested and compared in Section 4.1 with the classical BESO approach. Next, results on a three-material example are shown in Section 4.2, mainly demonstrating the convergence process, in particular the density regulation technique in convergence control. After this, results on a four-material example are also shown in Section 4.3, showing the effects of material properties on producing different optimal structures and the usage and necessity of using multi-material in structural design. Then, comparison between the proposed approach and the latest ordered SIMP approach [16] is given in Section 4.4, demonstrating its potentiality in producing structures of better targets. In the end, 3D examples under different numbers of candidate materials are shown. The computational time for the examples are summarized and compared in Table 1.

The 2D example mainly uses the classical MBB examples, under two different boundary conditions as described in Figs. 5(a) and 13(a), where the former is a half MBB example while the latter a full MBB example under symmetry requirement. The 3D example uses a classical Cantilever example in Fig. 16 as detailed later. Other optimization settings are also summarized below.

Initial value. As explained in Section 2, the proposed method is conducted in an evolutionary way via consequent mass deduction. The initial density value is set as a structure fully-filled with the material of the largest Young's modulus and density. The initial total mass constraint is the associated mass determined by the initial density.

Mass constraint. Unless a specific statement is made, mass constraint is represented by mass fraction M^c , defined by the ratio between a current mass M^* and the possible maximum mass M^{\max} , or $M^c = \frac{M^*}{M^{\max}}$.

Structural compliance and estimated compliance. Structural compliance C_{real} is the actual value of the optimized structure during each iteration step, while estimated compliance is the one computed as its approximation, or specifically $C_{iter} = \mathbf{c}(\mathbf{x}^i)^T \mathbf{x}^{i+1}$. The two values are compared during the optimization process in order to verify the results in Lemma 1. **Iteration gap.** In case of more-than-two materials, *step* refers to the step size in the iteration process as involved in the three sub-processing stages: preprocessing, upwards and downwards stages. The iteration step is set as $step = 0.3\%N$ in the following examples for efficiency without much changing the optimization result.

In the end, the evolutionary ratio $ER = 0.02$ and the filter $r_{min} = 2.5$ by default.

4.1. Two-material

The approach's effectiveness for two-material optimization problem is the most basic case, and also determines its performance in case of more than two materials. It is thus first tested

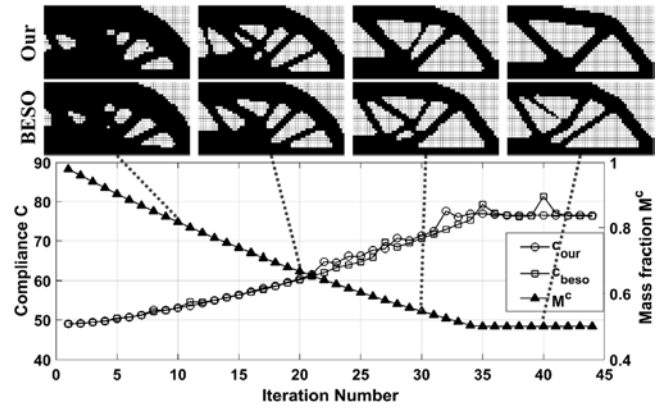


Fig. 6. Iteration histories of the compliance, mass constraint and topology at mass constraint $M^c = 0.5$. The solid material has ($E_A = 1, \rho_A = 1$), and the void element has ($E_{Void} = 0.001, \rho_{Void} = 0.001$). $c_{our} = 76.5, c_{beso} = 75.8$.

in this section on two cases: a special solid-void case, and a two-material case.

The example works on the half MBB beam in Fig. 5(a), consisting of 60×30 quadrilateral FE elements. The three involved testing materials A, B and Void, as shown in Fig. 5(b), are given as follows:

$$(E_A = 1, \rho_A = 1), (E_B = 0.2, \rho_B = 0.1),$$

$$(E_{Void} = 0.001, \rho_{Void} = 0.001). \quad (35)$$

The Young's modulus void element E_{Void} is set to be a small value to avoid producing singular stiffness matrix as widely used in previous studies in SIMP or BESO approaches. Its corresponding material density is also set to be a very small value in this mass constraint problem.

4.1.1. Solid-void materials

The proposed approach can work directly on the basic solid-void problem as a special case of two-material problem. Its performance is first shown in this section using the materials A and C described above, and compared with the benchmark results obtained via the classical discrete evolutionary approach BESO [2], as shown in Fig. 6. In these figures, the upper figures show the corresponding structures during the iteration at steps 1, 5, 15, 25, 35, 45, and the lower figures show the variation histories of the objective functions c_{our} for ours and c_{beso} for BESO method. The target mass $M^c = 0.5$, and both the proposed approach and the BESO gradually decrease the mass from the initial maximal one till the target, and thus share the same mass fraction curve in the figures. The BESO and the proposed approach demonstrate similar performance although BESO produces structure of slightly better compliance.

4.1.2. Two non-zero materials

The performance of two non-zero materials, using materials A and B described above under the mass constraint $M^c = 0.6$, was also tested, and the convergence histories was plotted in Fig. 7. Here, the produced structures as some key frames were also plotted on the top. As can be observed from the convergence histories in Fig. 7, the structural compliance increases initially as the mass fraction decreases, and then converges to an almost constant value after the objective mass is achieved. The final structure converges to a stable topology after 30 iterations; additional iteration steps are further plotted here to show its convergence.

We also compare the actual structural compliance C_{real} with the estimated compliance C_{iter} in Fig. 7, where c_{iter} shows bigger value

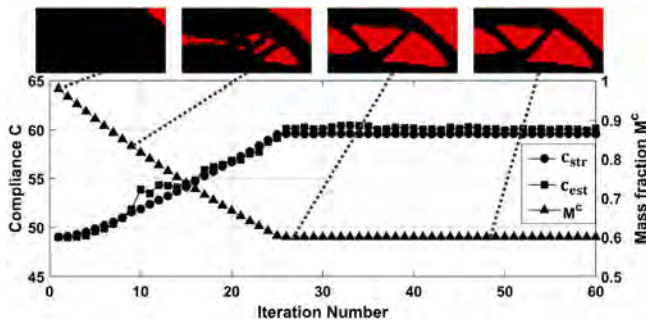


Fig. 7. Iteration histories of the compliance, mass constraint and topology for two materials ($E_A = 1, \rho_A = 1$), ($E_B = 0.2, \rho_B = 0.1$), at mass constraint $M^c = 0.6$. The compliance $C_{real} = 59.6$.

and less smooth convergence, but leads the iterative procedure to an expected structure. It comes to the objective value $C_{real} = 59.6$ and takes 2.1s for computation.

4.2. Three-material

Extending the two-material case to three-material case mainly involves an iterative searching for the best structure at the same mass constraint, which reducing from the initial maximal one to the target. The searching process involves additional steps of pre-processing, upwards, downwards searching stages, as explained in Section 3.2. Some important details will be further shown and explained in this section using a demonstrative three-material case on the same MBB example in Fig. 5. The target mass fraction $M_c = 0.3$, and the three materials A, B and C are shown in Fig. 5(c):

$$\begin{aligned} (E_A = 1, \rho_A = 1), (E_B = 0.6, \rho_B = 0.4), \\ (E_C = 0.01, \rho_C = 0.1). \end{aligned} \quad (36)$$

Two different iterations are involved in the optimization process: the *main-loop* each step of which produces an optimal structure at certain mass constraint, and the *sub-loop* at each main-loop step which searches for the best structure for all the possible candidate numbers of materials at a given mass constraint. The iteration details are shown in Fig. 8. The middle figure shows the main-loop while the four sub-figures around it shows sub-loop at each step of the main-loop. The sub-loop process consists of the preprocessing procedure, upwards and downwards searching procedures, each respectively represented by squares, upward-pointing and downward-pointing triangles. In addition, the inner iteration is controlled by the number of material A, and denoted by n_1 .

The sub-loop at each main step iteratively searches for the best structure at certain total mass constraint, where the produced structures are shown in each sub-figure. Each sub-loop produces an optimal structure and outlines it in a green box in the sub-figure. In order to improve the convergence stability, the produced structure was further optimized with a few additional steps using filters, and the produced associated structure was outlined in an orange box in the middle main figure. The produced nice structures also reveals the necessity and feasibility of the proposed density regulation process in ensuring convergence stability and in producing an optimal structure.

The variations of the associated volume and mass fraction of each material during the main iteration process were also plotted in Fig. 9. The quantities of different materials may vary in different directions until they together reach the optimal structure, of minimal compliance satisfying certain total mass constraint.

The proposed approach is also able to handle structures at high resolution, and it is demonstrated for the half MBB example in Fig. 5(a) using the following three kinds of materials:

$$(E_A = 1, \rho_A = 1), (E_B = 0.5, \rho_B = 0.4), (E_C = 0.01, \rho_C = 0.1). \quad (37)$$

The domain respectively consists of 60×30 and 200×100 square meshes, taking 31.2 s and 439.1 s to reach an optimal multi-material structure shown in Fig. 10(a), (b).

4.3. Four-material

The examples of four-materials are mainly designed for two purposes. The first is to test the effect of the number of candidate materials, and the effects of candidate materials in determining the final produced structures.

4.3.1. Effect of number of candidate materials

In order to test whether using a higher number of candidate materials will produce physical better structure, the MBB example in Fig. 5(a) was tested using the following four types of materials:

$$\begin{aligned} (E_A = 2, \rho_A = 1), (E_B = 1, \rho_B = 0.6), \\ (E_C = 0.6, \rho_C = 0.4), (E_D = 0.01, \rho_D = 0.1). \end{aligned} \quad (38)$$

The example was tested using various types of material combinations, using four, three and two candidate materials under the same total mass constraint $M^* = 900$. The produced structure for each type of material combination was shown in Fig. 11. The used candidate materials were indicated in the figures, and the associated structural compliances were shown in the figure captions. As can be observed from the results, the usage of more materials indeed produces structures of better compliance. In addition, it clearly shows the that usage of filter is able to remove unnecessary checkerboards and produces stable structures.

4.3.2. Effect of material properties

In order to further test the effect of the candidate material properties, for example the ranking of the Young's modulus or the modulus-density ratio, in determining the final produced structure, various different types of four-materials were tested and compared here. All the three cases are optimized by four candidate materials, while the material properties and target mass fraction are different, i.e. materials A, B, C and D are different in different cases. The produced structures were compared in Fig. 12.

In case 1, material A is much better than B and C, where $E_A > E_B > E_C$ and $E_A/\rho_A > E_B/\rho_B > E_C/\rho_C$, and the approach produces a structure composed by A and D only. In case 2, material B is the best in E/ρ , where $E_B/\rho_B > E_A/\rho_A > E_C/\rho_C > E_D/\rho_D$. However due to constraint of mass constraint and the Young's modulus $E_A > E_B > E_C > E_D$, the final produced structure is composed of materials A, B and D. In case 3, there are four irregular ladder-like materials, where $E_A > E_B > E_C > E_D$ and $E_A/\rho_A > E_B/\rho_B > E_C/\rho_C > E_D/\rho_D$, and all the four different materials were involved in the final produced structure. There is no clear evidence on the dependence of the final produced structure on property ranking of the materials.

4.4. Comparison with ordered SIMP

The problem of multi-material topology optimization under total mass constraint is only studied in previous work [21,16]. Comparison between the structures produced by the proposed approach and by the approach in [16] were conducted here. Note

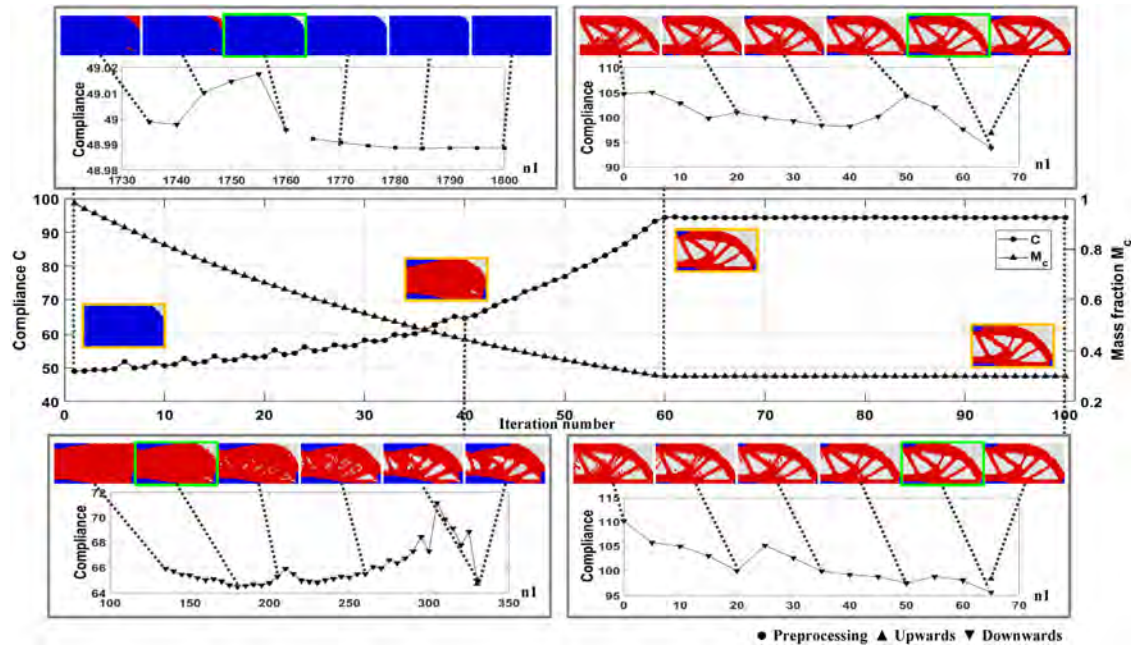


Fig. 8. Iteration process of a three-material problem, including sub-procedures. The middle figure shows the main-loop and the four sub-figures around it shows sub-loop at each step of the main-loop. The optimal structure in each sub-loop is outlined in green, which is then filtered (resulting in the structure outlined in orange) to improved convergence and used in the main-loop for next iteration. (For interpretation of the references to color in this figure legend, the reader is referred to the web version of this article.)

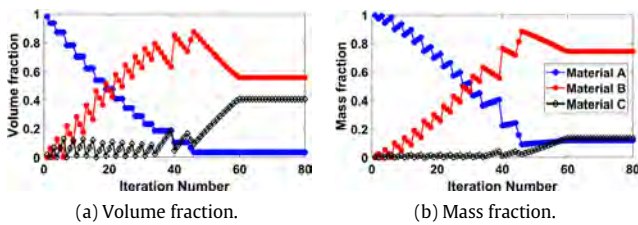


Fig. 9. History of variations of the volume and mass fraction of each material during the optimization procedure.

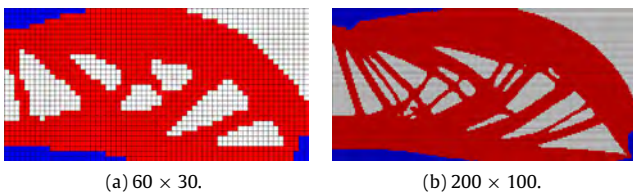


Fig. 10. An example of different meshing sizes.

also that the approach in [16] focuses on the multi-material optimization under *cost function* although the problem without the cost constraint is also studied. The totally same example proposed in [16] was tested, using the bridge example in Fig. 13(a) consisting of 100×50 square elements, imposed by unit external force F , and using four different types of candidate materials shown in Fig. 13(b). The target total mass fraction is $M^* = 0.4$.

The produced structures for the example are shown in Fig. 14, using four different cases of material combinations: (a) A, B, and C; (b) B and C; (c) A and C; and (d) C only. The cases (a)–(c) were solved using the recently proposed novel ordered-SIMP method in [16], whereas case (d) is solved using the classical SIMP method [29].

The optimal structures computed by ordered SIMP or SIMP were shown in the right column Fig. 14; similar results were also shown in [16]. Different candidate material combinations produced different optimal structures in these results almost using all the candidate materials. It is also interesting to observe that the structure produced using more types of materials may exhibit worse compliance than the structure produced using less types of materials. The unexpected cases were also observed by the authors in [16], demonstrating the challenges of multi-material topology optimization under total mass constraint. As comparison, the structures produced by the proposed approach were plotted in the left column in Fig. 14. All the final structures only consists of material C and the void, and they exhibiting better compliance than those produced by ordered SIMP, demonstrating the powerfulness of the proposed approach in detecting the optimal structures while avoids being stuck in local minima. The single-material optimal structure may be explained by the fact that material C has the largest stiffness–density ratio (E/ρ) among these four materials in Fig. 13(b), as noted in [16].

The convergence process of the proposed approach is also shown in Fig. 15. The Figs. 15(a) and 15(b) gives the results of the estimated compliances and of the actual structural compliances. We can observe that from the results that the estimated compliances produced in the three cases (optimized by more than two materials) show high similarity with the actual ones. In the case of single material, the estimated compliances different much with the actual one. However, the two cases still exhibits similar convergence trend, and ultimately produces a structural optimal structures. In addition, as can be seen from Table 1, given certain size of the problem, the calculation time of the ordered-SIMP approach just changes slightly when the number of candidate materials varies, while the proposed method is significantly impacted.

4.5. 3D examples

In this section, we investigate the performance of the proposed approach in 3D case using the 3D Cantilever beam in Fig. 16(a)

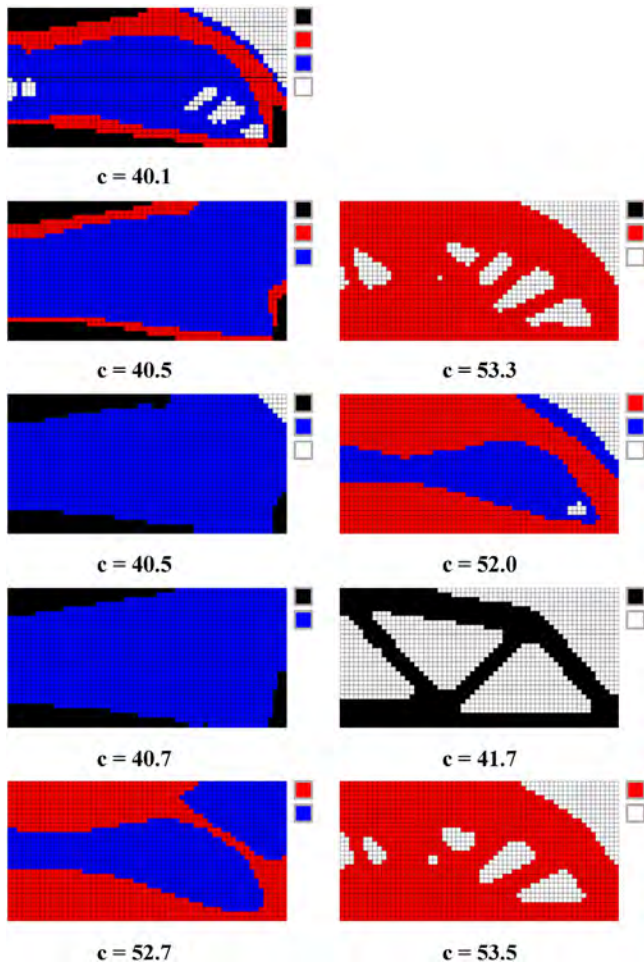


Fig. 11. Results of four-material optimization. The four materials are shown in black, red, blue and white, respectively, and c is the structure's compliance. (For interpretation of the references to color in this figure legend, the reader is referred to the web version of this article.)

under a sine-shaped load at the bottom of the free edge [30]. The design domain consists of $64 \times 24 \times 32$ FE elements. The multi-grid preconditioned conjugate gradients (MGCG) solver [30] is introduced here to reduce the computation cost and to speed up the calculation. The associated computation time is also summarized in Table 1. The derived optimal structures in case of two, three or four kinds of candidate materials are respectively shown in Figs. 16–18, where the used candidate materials, value of objective function and computing time are also described. Similar convergence performance was observed as that in 2D cases, which is not further explained here.

5. Conclusion

The paper proposes a novel approach using discrete variables to resolve the multi-material optimization problem under total mass constraint. The theoretical insights and the numerical techniques based on density regulations ensure a physical optimal structure produced. Performance of the approach was also tested on various numerical examples, using different types of material properties or using different number of candidate materials. In addition, the comparisons of the proposed approach with the latest approach [16] using ordered SIMP approach also demonstrates its capability in finding structures of a relative better compliance and in avoiding being stuck in local minima.

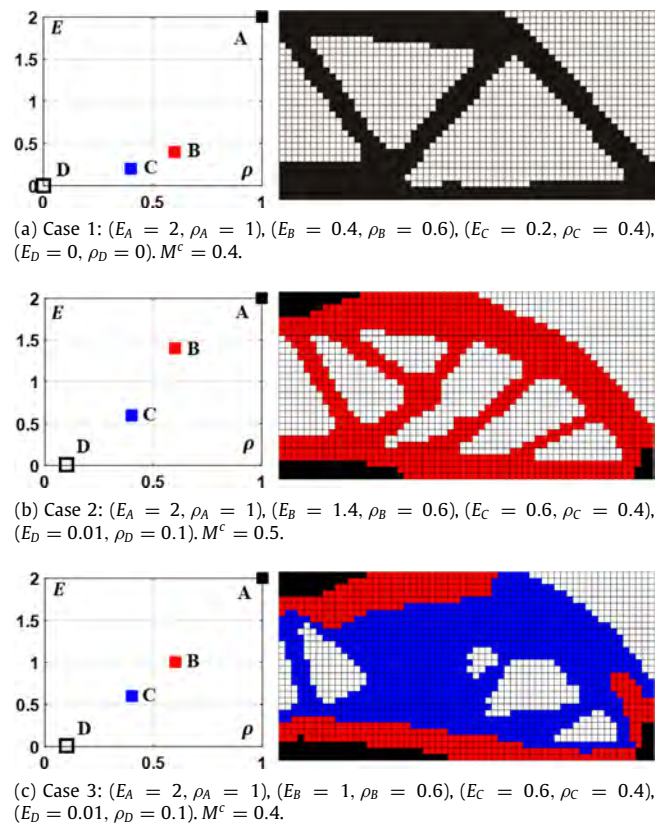


Fig. 12. An optimized structure may consist of different numbers of material types depending on the ranges of these materials, illustrated via a four-material optimization problem for the half MBB beam example.

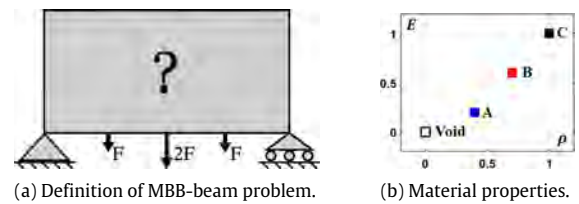


Fig. 13. Problem definition in Section 4.4.

Table 1

Summary of computation time (in seconds), including the 2D examples in Sections 4.1.1, 4.2, 4.4 and the 3D examples in Section 4.5. In the "SIMP/BESO*" row, * refers to the result by BESO, and the rest are by SIMP.

Problem	Size	M^c	m	Our	SIMP/ BESO*	Fig.
Half MBB	60×30	0.5	2	3.9	6.7*	6
		0.3	3	31.2	-	9(a)
	200×100	-	-	439.1	-	9(b)
MBB	100×50	0.4	4	422.9	172.2	14(a)
			3	346.5	165.3	14(b)
		0.7	3	345.5	174.0	14(c)
			2	11.4	138.5	14(d)
Cantilever	$64 \times 24 \times 32$	0.4	2	516.2	-	16
			3	2024.6	-	17
		0.7	4	6108.4	-	18

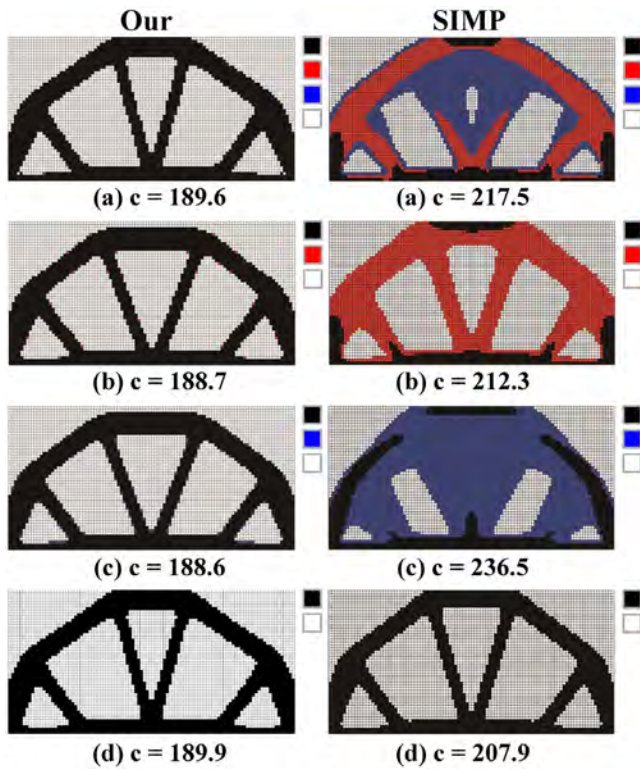


Fig. 14. Comparisons between the results produced by our approach and those produced by the latest ordered SIMP [16] using the examples proposed in [16] at mass fraction $M^c = 0.4$. The proposed approach is always able to produce structures of better objectives for all the different cases.

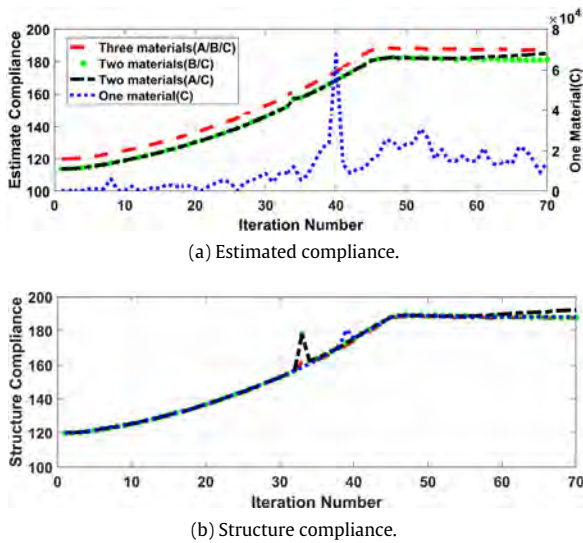


Fig. 15. Comparisons between the iteration history between the actual structural and the estimated compliance during optimization.

The present method is mainly limited to the traversal searching strategy in spite of its merit in producing a relatively better solution. Our future work is to develop an alternative efficient searching approach to overcome the limitation. In addition, it is interesting to note that the optimal structure in Fig. 14 only contains two materials instead of all the candidate materials. It deserves further research efforts to reveal the theoretical understanding behind the phenomenon. Our future work is also to extend the proposed

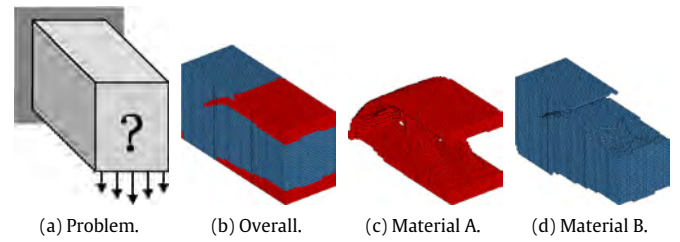


Fig. 16. A 3D Cantilever beam under a sine-shaped load at the bottom of the free edge using two kinds of candidate materials: $(E_A = 1, \rho_A = 1)$, $(E_B = 0.2, \rho_B = 0.1)$. The target total mass $M^c = 0.4$, and the derived structural compliance is 653.9.

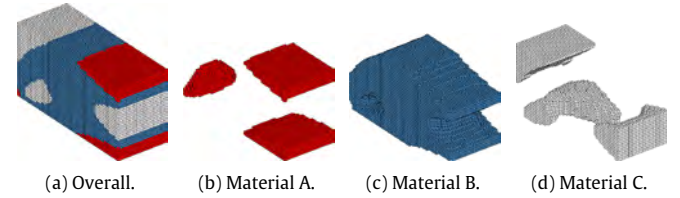


Fig. 17. Structure optimized under three kinds of candidate materials: $(E_A = 1, \rho_A = 1)$, $(E_B = 0.6, \rho_B = 0.4)$, $(E_C = 0.01, \rho_C = 0.1)$. The target total mass $M^c = 0.4$, and the derived structural compliance is 623.4.

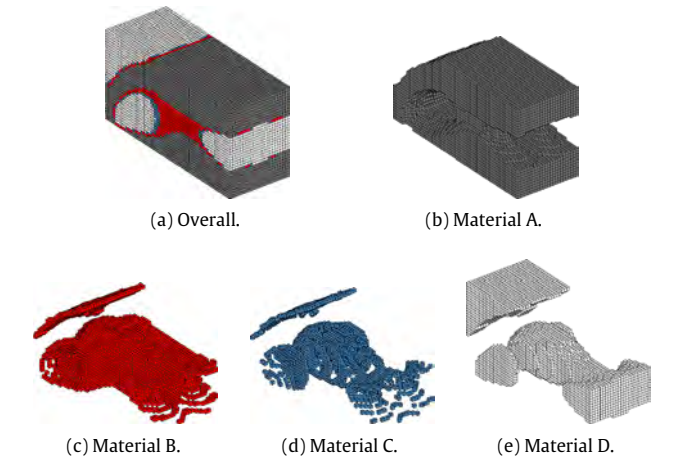


Fig. 18. Structure optimized by four kinds of candidate materials: $(E_A = 2, \rho_A = 1)$, $(E_B = 1.4, \rho_B = 0.6)$, $(E_C = 0.8, \rho_C = 0.4)$, $(E_D = 0.01, \rho_D = 0.1)$. The target total mass $M^c = 0.7$, and the derived structural compliance is 261.1.

approach to find the optimal multi-material microstructure, and to handle the cases of large deformations.

Acknowledgments

The work described in this paper is partially supported by the NSF of China (No. 61472356), and the National Key Research and Development Program (2016YFC1101302) from the MIST of China.

Appendix

Proof to Lemma 1 in Two-Material Situation. Suppose the numbers of elements filled with materials 1 and 2 are respectively n_1 and n_2 . Suppose the number of materials determined via the results in Lemma 1 gives strategy A, and another strategy B can be set as $n_1 - t$ and $n_2 + t$, for $t \in \mathbb{Z}^+$ and $0 \leq n_1 - t, n_2 + t \leq N$. Let

$$Q(f, n_1^f, n_2^f) = \mathbf{c}(\mathbf{x}^0)^T \mathbf{x}_f, f = A, B, \tag{39}$$

where the numbers of material 1,2 is respectively n_1^f and n_2^f .

We can see from the results obtained by strategies A and B,

$$\begin{aligned} Q(f_A, n_1^A, n_2^A) &= E_1 \sum_{i \in A_1} c_i + E_2 \sum_{i \in A_2} c_i, \\ Q(f_B, n_1^B, n_2^B) &= E_1 \sum_{i \in B_1} c_i + E_2 \sum_{i \in B_2} c_i \end{aligned} \quad (40)$$

where $A_j, B_j, j = 1, 2$ are the sets of sequence numbers whose corresponding element are filled by material j .

Apparently, there is

$$n_1^A = n_1, \quad n_2^A = n_2, \quad n_1^B = n_1 - t, \quad n_2^B = n_1 + t, \quad (41)$$

$$\begin{aligned} A_1 &= \{1, \dots, n_1\}, & A_2 &= \{n_1 + 1, \dots, N\}, \\ B_1 &= \{1, \dots, n_1 - t\}, & B_2 &= \{n_1 - t + 1, \dots, N\}. \end{aligned} \quad (42)$$

Taking (41), (42) into (40) gives

$$\begin{aligned} &Q(f_A, n_1, n_2) - Q(f_B, n_1 - t, n_2 + t) \\ &= E_1 \left(\sum_{i \in A_1} c_i - \sum_{i \in B_1} c_i \right) \\ &\quad + E_2 \left(\sum_{i \in A_2} c_i - \sum_{i \in B_2} c_i \right) \\ &= E_1 \left(\sum_{i \in A_1 \cap B_2} c_i - \sum_{i \in A_2 \cap B_1} c_i \right) \\ &\quad + E_2 \left(\sum_{i \in A_2 \cap B_1} c_i - \sum_{i \in A_1 \cap B_2} c_i \right) \\ &= (E_1 - E_2) \left(\sum_{i \in A_1 \cap B_2} c_i - \sum_{i \in A_2 \cap B_1} c_i \right). \end{aligned} \quad (43)$$

Since

$$\begin{aligned} N_{A_1 B_2} &= |A_1 \cap B_2| = |A_1| - |A_1 \cap B_1|, \\ N_{A_2 B_1} &= |A_2 \cap B_1| = |A_2| - |A_1 \cap B_1|, \end{aligned} \quad (44)$$

$$\begin{aligned} c_{A_1 B_2}^{\min} &= \min\{c_i | i \in A_1 \cap B_2\}, \\ c_{A_2 B_1}^{\max} &= \max\{c_i | i \in A_2 \cap B_1\}, \end{aligned} \quad (45)$$

and

$$N_{A_1 B_2} \geq N_{A_2 B_1}, \quad c_{A_1 B_2}^{\min} \geq c_{A_2 B_1}^{\max}, \quad (46)$$

we have from (43) that

$$\begin{aligned} &Q(f_A, n_1, n_2) - Q(f_B, n_1 - t, n_2 + t) \\ &= (E_1 - E_2) \left(\sum_{i \in A_1 \cap B_2} c_i - \sum_{i \in A_2 \cap B_1} c_i \right) \\ &\geq (E_1 - E_2) (N_{A_1 B_2} \cdot c_{A_1 B_2}^{\min} - N_{A_2 B_1} \cdot c_{A_2 B_1}^{\max}) \\ &\geq (E_1 - E_2) (N_{A_1 B_2} - N_{A_2 B_1}) \cdot c_{A_2 B_1}^{\max} \\ &\geq 0 \end{aligned} \quad (47)$$

which means it is always verified that $\mathbf{c}(\mathbf{x}^0)^T \mathbf{x}_A \geq \mathbf{c}(\mathbf{x}^0)^T \mathbf{x}_B$. \square

References

- [1] Bendsoe M, Kikuchi N. Generating optimal topologies in structural design using a homogenization method. *Comput Methods Appl Mech Engrg* 1988;72(2):197–224.
- [2] Huang X, Xie YM. *Evolutionary Topology Optimization of Continuum Structures: Methods and Applications*. Wiley; 2010.
- [3] Sigmund O, Maute K. Topology optimization approaches: a comparative review. *Struct Multidiscip Optim* 2013;48(6):1031–55.
- [4] van Dijk NP, Maute K, Langelaar M, van Keulen F. Level-set methods for structural topology optimization: a review. *Struct Multidiscip Optim* 2013;48(3):437–472.
- [5] Xia L, Xia Q, Huang X, Xie YM. Bi-directional evolutionary structural optimization on advanced structures and materials: A comprehensive review. *Arch Comput Methods Eng* 2016;1–42.
- [6] Niemann S, Kolesnikov B, Hhne C, Querin O, Toropov V. The use of topology optimisation in the conceptual design of a next generation lattice composite fuselage structure, in: *Aircraft Structural Design Conference*, 2012.
- [7] Zhu JH, Zhang WH, Xia L. Topology optimization in aircraft and aerospace structures design. *Arch Comput Methods Eng* 2015;1–28.
- [8] Bendsoe M. Optimal shape design as a material distribution problem. *Struct Optim* 1989;1(4):193–202.
- [9] Allaire G, Jouve F, Toader AM. A level-set method for shape optimization. *C. R. Math.* 2002;334(12):1125–30.
- [10] Wang MY, Wang X, Guo D. A level set method for structural topology optimization. *Comput Methods Appl Mech Engrg* 2003;192(1–2):227–46.
- [11] Mattheck C, Burkhardt S. A new method of structural shape optimization based on biological growth. *Int J Fatigue* 1990;12(3):185–90.
- [12] Young V, Querin OM, Steven GP, Xie YM. 3D and multiple load case bi-directional evolutionary structural optimization (BESO). *Struct Multidiscip Optim* 1999;18(2):183–92.
- [13] Svanberg K, Werme M. Sequential integer programming methods for stress constrained topology optimization. *Struct Multidiscip Optim* 2007;34(34):277–299.
- [14] Rozvany GIN. A critical review of established methods of structural topology optimization. *Struct Multidiscip Optim* 2009;37:217–37.
- [15] Gibson RF. A review of recent research on mechanics of multifunctional composite materials and structures. *Compos Struct* 2010;92(12):2793–810.
- [16] Zuo W, Saitou K. *Multi-Material Topology Optimization using Ordered SIMP Interpolation*. Springer-Verlag New York, Inc.; 2017.
- [17] Tavakoli R. Multimaterial topology optimization by volume constrained allenchahn system and regularized projected steepest descent method. *Comput Methods Appl Mech Engrg* 2014;276(7):534–65.
- [18] Tavakoli R, Mohseni SM. Alternating active-phase algorithm for multimaterial topology optimization problems: a 115-line Matlab implementation. *Struct Multidiscip Optim* 2014;49(4):621–42.
- [19] Park J, Sutradhar A. A multi-resolution method for 3d multi-material topology optimization. *Comput Methods Appl Mech Engrg* 2015;285(2):571–86.
- [20] Wang MY, Zhou S. Color level sets: a multi-phase method for structural topology optimization with multiple materials. *Comput Methods Appl Mech Engrg* 2004;193:469–96.
- [21] Ramani A. Multi-material topology optimization with strength constraints. *Struct Multidiscip Optim* 2011;43(5):597–615.
- [22] Huang X, Xie YM. Bi-directional evolutionary topology optimization of continuum structures with one or multiple materials. *Comput Mech* 2008;43(3):393.
- [23] Sigmund O. A 99 line topology optimization code written in Matlab. *Struct Multidiscip Optim* 2001;21(2):120–7.
- [24] Gao T, Zhang W. A mass constraint formulation for structural topology optimization with multiphase materials. *Internat J Numer Methods Engrg* 2011;88(8):774–96.
- [25] Gao T, Xu P, Zhang W. Topology optimization of thermo-elastic structures with multiple materials under mass constraint. *Comput Struct* 2016;173:150–60.
- [26] Sanders ED, Aguiló MA, Paulino GH. Multi-material continuum topology optimization with arbitrary volume and mass constraints. *Comput Methods Appl Mech Eng* 2018.
- [27] Xia L, Xia Q, Huang X, Xie YM. Bi-directional evolutionary structural optimization on advanced structures and materials: a comprehensive review. *Arch Comput Methods Eng* 2016;1–42.
- [28] Huang X, Xie YM. Evolutionary topology optimization of geometrically and materially nonlinear structures under prescribed design load. *Struct Eng Mech* 2010;34(5):581–95.
- [29] Andreassen E, Clausen A, Schevenels M, Lazarov BS, Sigmund O. Efficient topology optimization in Matlab using 88 lines of code. *Struct Multidiscip Optim* 2011;43(1):1–16.
- [30] Amir O, Aage N, Lazarov BS. On multigrid-CG for efficient topology optimization. *Struct Multidiscip Optim* 2014;49(5):815–29.